

FaceTopoNet: Facial Expression Recognition using Face Topology Learning

Mojtaba Kolahdouzi, Alireza Sepas-Moghaddam, *Member, IEEE*, and Ali Etemad, *Senior Member, IEEE*

Abstract—Prior work has shown that the order in which different components of the face are learned using a sequential learner can play an important role in the performance of facial expression recognition systems. We propose FaceTopoNet, an end-to-end deep model for facial expression recognition, which is capable of learning an effective tree topology of the face. Our model then traverses the learned tree to generate a sequence, which is then used to form an embedding to feed a sequential learner. The devised model adopts one stream for learning structure and one stream for learning texture. The structure stream focuses on the positions of the facial landmarks, while the main focus of the texture stream is on the patches around the landmarks to learn textural information. We then fuse the outputs of the two streams by utilizing an effective attention-based fusion strategy. We perform extensive experiments on four large-scale in-the-wild facial expression datasets - namely AffectNet, FER2013, ExpW, and RAF-DB - and one lab-controlled dataset (CK+) to evaluate our approach. FaceTopoNet achieves state-of-the-art performance on three of the five datasets and obtains competitive results on the other two datasets. We also perform rigorous ablation and sensitivity experiments to evaluate the impact of different components and parameters in our model. Lastly, we perform robustness experiments and demonstrate that FaceTopoNet is more robust against occlusions in comparison to other leading methods in the area.

Impact Statement—Systems that perform facial expression recognition (FER) have a wide variety of applications in real-world problems such as human-machine interaction, robotics, mental health management systems, to name but a few. Our proposed solution achieves better recognition rates in comparison to many other methods in the field of FER, allowing for development of more accurate systems. Moreover, our proposed method demonstrates more robustness against occlusions, which can be beneficial for in-the-wild scenarios. Lastly, our model can learn trees that are optimized, yet also generalize well across different datasets and perform considerably better than human-designed face trees.

Index Terms—Face graphs, facial expression recognition, tree topology learning

I. INTRODUCTION

This work was funded by Irdeto Canada Corporation and the Natural Sciences and Engineering Research Council of Canada (NSERC).

Mojtaba Kolahdouzi is a Ph.D. student in the Department of Electrical and Computer Engineering and Ingenuity Labs Research Institute at Queen's University, Kingston, Canada (19mk73@queensu.ca)

Alireza Sepas-Moghaddam is a research collaborator in the Department of Electrical and Computer Engineering and Ingenuity Labs Research Institute at Queen's University, Kingston, Canada (alireza.sepasmoghaddam@queensu.ca)

Ali Etemad is an Associate Professor and a Mitchell Professor in AI for Human Sensing and Understanding, in the Department of Electrical and Computer Engineering and Ingenuity Labs Research Institute, at Queen's University, Canada. (e-mail: ali.etemad@queensu.ca)

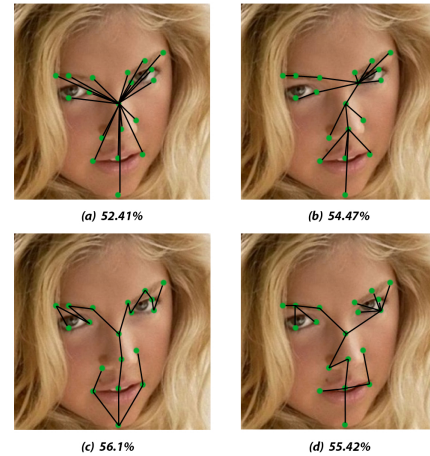


Fig. 1: A face image together with 4 random trees. Associated recognition rates are shown beneath each image.

FACIAL expressions play a key role in conveying a wide range of human emotions [1], [2]. Thus, considerable attention has been given to automatic facial expression recognition (FER) using machine learning and deep learning methods, where the goal is to identify different expressions from images or videos of the face [3]–[5]. Recent progress in deep neural networks and computational resources, along with the availability of vast amounts of data, have resulted in great progress in the area of FER [6]. Applications of FER include but are not limited to emotion classification [4], pain intensity detection [7], age estimation [8], estimation of the user's experience during consumption of multimedia content [9], and detection and prediction of the severity of depression [10], among many others. A detailed recent review of FER is presented in [11].

While many early deep FER approaches such as [12] and [13] focused on *holistic* representations of the face, many newer methods have shifted focus to *part-based* approaches to describe the face as distinct [14] or disentangled components [15]. The reason for this focus toward part-based methods is that certain regions of the face such as mouth or periorcular areas have been shown to play different roles in reflecting different expressions [16]. Part-based FER techniques typically analyze face regions separately to extract local features, which are then merged to produce global representations [14]. As a result, given that graph-based methods generally lend themselves well to part-based problems, they have recently gained popularity for FER [17]–[22]. In such approaches, each node in a graph can be associated with

a facial region, where an edge can reflect the connections or relationships between the regions, for instance their joint movement or distance.

Despite the fact that a number of graph-based FER methods have shown promising results [18], [23], the underlying graph topology used to learn the structure of the face is not generally agreed upon. In other words, there is no single way of knowing how various face regions should be connected such that the model’s performance would be maximized. Graph-based FER methods assume the topology of underlying graphs as being either fully-connected [18], [19], [21] or partially-connected [17], [20], [22]. In the fully-connected scenario, one must add $\binom{n}{2}$ edges to the underlying graph, which makes the training process cumbersome. Additionally, some of the edges are unnecessary within the graph, which may cause overfitting. In the partially-connected scenario, in light of the fact that the topology is pre-defined and engineered as opposed to being learned, it may not include the optimal or near-to-optimal edges between face regions. In any case, the underlying graph topology can significantly impact the performance of any subsequent learner that adopts the information obtained from different facial regions toward part-based FER. As an example Figure 1 depicts a face image together with 4 random trees which have been used to connect different regions of the face. Traversal of the trees yields 4 distinct sequence-based embeddings, using which we can conduct a 7-class FER task using 4 independent sequential learners (long short-term memory (LSTM) has been used in this case). The associated recognition rates (RR) are provided beneath each image in the Figure 1, where we observe a 3.7% variance, demonstrating the necessity of selecting the optimal tree topology.

In this paper, we present an end-to-end pipeline, FaceTopoNet, that learns an effective tree of the face for robust FER in a deep neural architecture. First, we assume a weighted fully-connected graph obtained from facial landmarks, which is then optimized by an evolutionary algorithm [24]. This graph is then used to form a minimum-cost spanning tree, the traversal of which forms a sequence of facial nodes. This sequence is then used for two subsequent streams, which we name *texture* and *structure* streams. In the structure stream, the obtained sequence is used to feed a sequential learner followed by soft attention to focus on the salient cells of the learner. In parallel, in the texture stream, we apply local patches around each of the extracted nodes and encode each region using a simple ConvNet. These encoded representations are used to feed a sequential learner similar to the structure stream, followed by soft attention. The final embeddings of the two streams are then fused for final expression recognition. To the best of our knowledge, our work is the first to optimize the relevant order of facial regions for sequential learning in the context of FER. We perform rigorous experiments on four in-the-wild large-scale FER datasets, AffectNet [25], FER2013 [26], RAF-DB [27], and ExpW [28], and one lab-controlled dataset, i.e. CK+, to illustrate the efficacy of our devised method. Our method outperforms the state-of-the-art results on three of the datasets and achieves competitive results on the other two. We further perform additional experiments on ablations and even evaluate the robustness of our method to occlusions in

different key regions of the face.

our contributions are three-fold. (1) We propose a novel end-to-end deep architecture to identify and use the effective tree topologies for FER. These face trees are found by using the idea of weighted complete graphs and minimum-cost spanning trees. They are then used to determine the input order of the embeddings to be fed to two sequential learners located in two separate streams responsible for learning the structure and texture of the face. (2) Our experiments demonstrate the strong performance of our method by setting new state-of-the-art results on AffectNet, FER2013, and ExpW, and performs competitively on RAF-DB and CK+. (3) Our solution is robust to different occlusions added to input images. Further, we find that our method automatically adapts and finds different face trees for each dataset, and uses them to obtain improved performance. It is worth mentioning that in traditional landmark-based methods the input order of the sequential learner is not learned as opposed to FaceTopoNet. In fact, FaceTopoNet provides a way to simultaneously learn the input orderings of a sequential learner and its free parameters.

This paper is an extension of our prior work [29] which has been published in FG 2021 as a short paper. In comparison, this paper adds the followings: (i) We use three additional publicly available datasets, namely RAF-DB, ExpW, and CK+, to evaluate the proposed method. (ii) We analyze and discuss the effects of using different sequential learners and encoders with different pre-trainings. (iii) We perform robustness experiments toward occlusions against other state-of-the-art methods by manually removing different key regions of the face. (iv) We study the effect of different patch sizes which are located around the facial landmarks on the overall recognition rates. (v) The effects of the number of extracted facial landmarks is studied (vi) We perform a cross-dataset study utilizing face trees. (vii) Lastly, we perform a direct comparison between the *learned* face trees and prior human-defined trees used for FER.

The rest of this paper is organized as follows: Section II provides a summary of the related work in the field. The proposed method including the detailed description of tree topology learning is given in section III. Section IV presents the results of the extensive experiments along with the detailed ablation analysis, and finally section V concludes the paper.

II. RELATED WORK

FER systems can be divided into static and dynamic categories with respect to the type of input data [11]. In static-based methods, the facial features are encoded based on the spatial information available in a *single* image, whereas dynamic-based methods additionally exploit the temporal relationships between adjacent frames available in the input *video*. Our focus in this paper lies in the first category. Hence, we review relevant papers for image-based FER in this section. Additionally, given the use of graphs in our method, we provide a review of the available techniques that incorporate graph theory in FER systems.

A. FER with Deep Learning

In one of the early neural network-based methods for FER, a shallow CNN was used for feature learning, followed by a linear support vector machine (SVM) for classification [30]. Another method, HoloNet, was introduced in [31], combining residual structures with concatenated rectified linear activation scheme [32]. In addition, an inception-residual structure was adopted in the final layers to enable multi-scale feature extraction. In [33], a nine-layer CNN with a multi-class SVM classifier was used for FER.

In [15], the notion of disentanglement was used to make FER systems more robust against pose, illumination, and other variations. In this context, a radial metric learning strategy was proposed for disentangling identity-specific factors from facial input images. In [34], an attention method was proposed to selectively focus on facial muscle moving regions. To guide the attention learning process, prior domain knowledge was incorporated by considering the differences between neutral and expressive faces during training. In [35], another attention-based method was suggested. The method used a region-attention network to identify the importance of different facial regions for FER, thus assigning higher weights to facial regions with greater importance. This resulted in further robustness to occlusions and pose variations.

In [36], the so called advanced softmax loss was proposed to reduce the negative effects caused by data imbalance, particularly when the classifier is biased toward the majority class. In [37], the authors synthesized facial affects from a neutral image for data augmentation in FER systems. Their model accepts a neutral image and a basic facial expression as inputs and fits a 3D Morphable model [38] to the neutral image, deforming it for adding the expression. A model called MA-Net was proposed in [39] for conducting in-the-wild FER. The proposed solution includes three components. In the first component, named feature pre-extractor, mid-level features of face images are extracted. The second component tries to fuse different features which are related to different receptive fields, and finally in the third component, the network is guided to be more focused on the more important local features. A model named TransFER was proposed in [40] for FER. The approach is capable of learning complex local representations and is comprised of three sub-networks: (i) multi-attention dropping, forcing the model to come up with more diverse local patches; (ii) vision transformer to model the relations existing among different local patches; and (iii) multi-head self-attention dropping which drops a self-attention module randomly to make the model learn different local patches in a diverse way.

Since facial attributes which are associated with identity, like race or age, can hinder the efficacy of FER systems, an identity-free FER system is proposed in [41]. The authors have made use of a generative adversarial network to transform a given face image with a specific identity to its “average” identity version while preserving the same expression. A new way to view the facial expressions was proposed in [42]. Specifically, the authors utilized a feature decomposition network to extract shared information among expressions and a

feature reconstruction network to extract expression-specific information. In [43], for data augmentation purpose, the authors used StarGAN [44] to synthesize identity-specific face images with basic emotions. Then, a deep network was used to extract latent embeddings from both synthesized and real images. These embeddings were used to train a Mahalanobis metric network for performing FER. In [45], the authors design a FER system to assist healthcare systems. In this regard, they propose different convolutional neural network architectures to handle multiresolution facial images. Hossain *et al.* in [46] propose a three-component FER system. First component includes the detection of facial regions, the second component uses CNNs to extract the embeddings, and the third component adopts different techniques like transfer learning to extract more distinctive embeddings. A novel data augmentation technique is introduced in [47] for performing FER. This technique includes applying edge enhancement filters like bilateral filtering on the images. Although deep learning methods provide the state-of-the-art results in FER, some papers like [48] use a conventional machine learning approach (feature extraction, feature classification, and classification) to perform FER and achieved reasonable results.

In [49], a novel residual-based CNN architecture, Bounded Residual Gradient Network (BReG-Net), was proposed for FER. This CNN architecture includes 39 layers of residual blocks, where the standard skip-connections in the ResNet blocks were replaced by a differentiable function with a bounded gradient, thus avoiding the gradient vanishing and exploding problems. As an extension to [49], the same authors proposed BReG-NeXt in [50], which includes more trainable parameters and offers more flexibility. A trainable parameter has also been added to the residual units. While this complex mapping adds few more parameters to each residual block, it extracts more representative features in comparison to its counterparts like ResNet-50.

B. Applications of Graphs in FER

Neural networks on graph topologies have recently gained momentum for visual analysis tasks [51], [52], including FER [17]–[20]. In [19], Gabor features were first extracted from texture information around 49 facial landmarks and were then combined with the Euclidean distances calculated between landmark pairs to feed a bidirectional gated recurrent unit. In [18], local regions around five landmarks, including center of left and right eyes, nose, and left and right mouth corners, were extracted to be then learned using a GCN. Similarly in [21] 28 landmarks corresponding to eyebrows and mouth were selected to create three separate graphs for left/right eyebrows and mouth. These graphs were then processed using a graph temporal convolutional network. In [20], 34 landmarks, corresponding to three facial components including left eye and eyebrow, right eye and eyebrow, and mouth, were first detected and the connections between these components were established with respect to their psychological semantic relationships. Histogram of orientation features and the XY coordinates of the nodes were then combined to feed a spatial-temporal semantic graph network. A novel multi-task learning

was proposed in [53], which adopted GCNs to model the dependencies among the discrete and continuous models of emotions. To be more specific, a shared representation was learned for both discrete and continuous models of emotion, and the final classifier of the discrete model and the regressor of the continuous model were jointly learned through a GCN. In [54], the authors adopted a GCN into a well-known CNN-RNN based model for performing FER. The role of the GCN was to help the model learn more salient features. Additionally, an LSTM layer was utilized to learn long dependencies between the GCN-extracted features.

Unlike all these techniques which employ fully connected graphs for FER, a few solutions such as [20] and [17] assume a pre-defined subset of connections between the nodes followed by a variation of graph convolutional networks. Nonetheless, to the best of our knowledge, all the graph-based FER solutions utilize a pre-defined graph topology (whether fully connected or otherwise) to be then used for every scenario. The problem with these pre-defined graphs is that they do not necessarily include the optimal set of connections, and once designed, stay unchanged for different datasets. We aim to tackle this problem by proposing a novel pipeline in which a unique effective tree topology can be learned given the problem space.

III. PROPOSED METHOD

A. Problem Setup and Solution Overview

Graphs can be used to model the topology and the relationship between different facial landmarks. Each vertex in these graphs can represent a facial landmark, while the existence of an edge between two vertices (facial landmarks) would consequently demonstrate that there is a relationship between the two. In [55], it was shown that these graphs provide a better representation when compared to holistic approaches. The constructed graphs can then be processed using deep networks like 3D-CNNs [56], GCNs [57], or RNNs [19] (which we refer to as *sequential learners*) [58]. As shown in Figure 1, when using a sequential learner, the accuracy of a solution can be affected by the topology of the graph being processed. Nonetheless, to the best of our knowledge, no technique for learning the topology of graphs for FER has been previously proposed in the literature.

To address the aforementioned problem, we propose a new solution in this paper to learn the topology of the graph in the form a face tree, and then use this tree to further learn effective representations from the face.

In our designed solution, for learning the salient information of the face, two important streams are considered: *structure* and *texture*. The backbone of these two streams are two sequential learners. Accordingly, our proposed end-to-end method uses the spatial information of the extracted facial landmarks in the structure stream and the texture information of the patches around these facial landmarks in the texture stream. The final embeddings to be fed into the sequential learners are determined by the topology of the learned face tree. In other words, we traverse the face tree to generate a sequence, and this sequence determines the ordering of the embeddings to be fed into the sequential learners. Our

proposed pipeline’s architecture is depicted in Figure 2. What follows is the detailed description of our tree topology learning procedure along with the two-stream solution.

B. Tree Topology Learning

First, we employ a landmark extractor Φ to detect facial landmarks from an input image I such that:

$$\lambda = \Phi(I), \quad (1)$$

where $\lambda = [\lambda_1 \cdots \lambda_i \cdots \lambda_n]$, λ_i represent the coordinates of the i th facial landmark in Euclidean space, and n is the number of extracted facial landmarks. The optimal value of n will be studied in the experiments section. In this work, we use a deep regression architecture [59] as $\Phi(\cdot)$. Next, we suppose that the extracted facial landmarks are vertices of a graph. We thus have a graph with n vertices where each vertex represents a facial landmark. We then add all the possible edges, obtaining a complete graph K_n .

Next, an optimization algorithm (described below in this section) assigns weights to the edges of K_n , making it a weighted complete graph. Following, we extract a minimum-cost spanning tree from K_n . This minimum-cost spanning tree can be expressed as:

$$MST = \{(V_{MST}, E_{MST})\}, \quad (2)$$

where MST is the minimum-cost spanning tree, and V_{MST} and E_{MST} represent the vertices and edges of MST , respectively. Here, $V_{MST} = V_{K_n}$, $E_{MST} \subset E_{K_n}$, where V_{K_n} and E_{K_n} denote the vertices and edges of K_n . Moreover, in this setup, $\sum_{\forall e_{ij} \in E_{MST}} e_{ij}$ is minimum. For finding MST , we use Algorithm 1 based on [60].

By utilizing the MST , we aim to generate a sequence which determines the ordering of the embeddings for both structure and texture streams. The reason behind converting the complete graph K_n to a tree is that trees are acyclic in nature and are thus better suited for sequence formation. For the purpose of sequence formation, we traverse MST using the preorder depth first algorithm described in [61]. In the context of our problem, we start the MST traversal from the most centered vertex, i.e., nose tip. Ultimately, a sequence of vertices is built. We depict the tree traversal in Figure 3. In this figure, for a clear visualization, we explain the process for a tree with only $n = 9$ nodes instead of the entire set of landmarks.

Suppose that the sequence generated after the tree traversal is denoted by $v = [v_1 \cdots v_\gamma]$, where v_1 is the first vertex (landmark) of the tree, and γ is one of the existing vertices between 1 and n . Accordingly, the number of elements in vector v is provably $2n - 1$. By utilizing v , we build matrix $U = [u_1 \cdots u_\gamma]$, where u_1 is a vector whose elements are zeros except for the first element. Similarly, u_γ is a vector whose elements are zeros except for the γ^{th} element. Matrix U is then used to generate the input embeddings of the sequential learners, which will be described in Section III-C.

To learn an effective face tree structure, the weights of K_n need to be updated. In other words, changing the weights of K_n results in different face trees, thus different sequences.

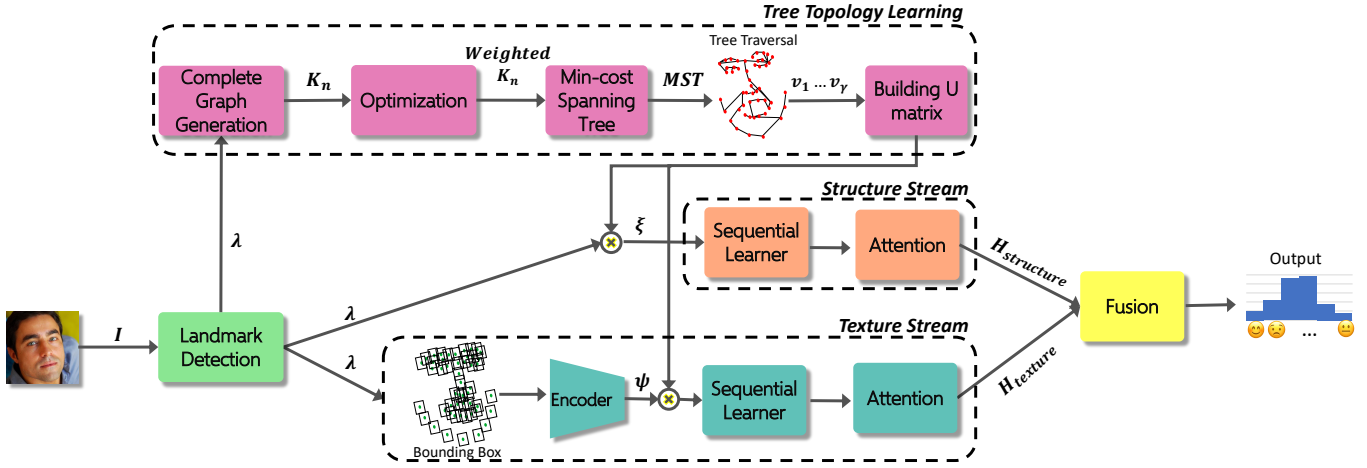


Fig. 2: The pipeline of the proposed FaceTopoNet.

Algorithm 1: Minimum cost spanning tree

Result: MST

Initialization: $visited = \{i\}$,

$unvisited = \{0, 1, \dots, i-1, i+1, \dots, \binom{n}{2}\}$, $MST = \emptyset$

while $unvisited \neq \emptyset$ **do**

find edge $e = (P, Q) \ni P \in visited$ and
 $Q \in unvisited$ and e has the smallest weight
 $MST = MST \cup \{e\}$
 $visited = visited \cup \{Q\}$
 $unvisited = unvisited - \{Q\}$

end

Given the greedy nature of Algorithm 1, it is difficult to express the output of our pipeline as a differentiable function of the weights of K_n . In dealing with such problems, various optimization algorithms can be used to learn effective trees. In this work, we utilize the Cooperatively Coevolving Particle Swarms for Large Scale Optimization (CCPSO2) algorithm [24], which is an evolutionary method, to optimize the weights of K_n . CCPSO2 belongs to a family of meta-heuristic cooperative algorithms, which makes use of swarm intelligence as well as their cooperation to estimate the solution of optimization problems of up to 2000 variables effectively [24]. Due to the fact that our search space in this work has $\binom{n}{2}$ dimensions, for a reasonably constrained value such as $n = 50$, CCPSO2 can perform effectively for this problem. We use this optimization technique to learn the weights of K_n while minimizing the loss function of the model \mathcal{L}_{total} , which we will define later in Section III-F. It is worth mentioning that while CCPSO2 does not promise an optimal solution (it can get stuck in local optima like many other optimizers), what matters is the generalization ability of the converged face tree on unseen data, which will be extensively tested on 5 different FER datasets in the experiment section of the paper.

C. Structure Stream

Here, we aim to learn a sequential learner by using the spatial information of the extracted facial landmarks. Specifically, the input embedding of this sequential learner is determined by the matrix U . As shown in Figure 2, the inputs to the structure stream are the matrix λ which contains the spatial information of the facial landmarks, together with the U matrix. These two matrices are used to form the input embedding for the sequential learner, for example an LSTM with peephole connections [62]. The input embedding ζ is generated by:

$$\zeta = \lambda \times U. \quad (3)$$

An LSTM network consists of a number of cells, the output of which continuously evolves with regards to its memory content. Moreover, each cell has a common cell state which is necessary for keeping track of long-term dependencies within the LSTM network. Two gates control the flow of information in the common cell state: input and forget gates, which make the LSTM cell decide when to forget or update the cell's state. The output of an LSTM cell is its hidden state, which is also controlled by the common cell state. We input ζ to the LSTM network and the aggregation of hidden states makes the final output of the LSTM network.

Next, we incorporate an attention mechanism [63] over the output of our sequential learner to focus on the salient parts of the embedding. To do so, each hidden state vector of the sequential learner cell (h_i) is multiplied by a learnable weight δ_i . δ_i controls the amount of attention each h_i receives and can be expressed as:

$$\delta_i = \frac{e^{o_i}}{\sum_{k=1}^n e^{o_k}}, \quad (4)$$

where n illustrates the number of units in the sequential learner and o_i can be calculated using the following equation:

$$o_i = \tanh(W_h h_i + b_h). \quad (5)$$

Here, W_h and b_h denote the set of trainable weights and biases respectively. We calculate the final attentive output of

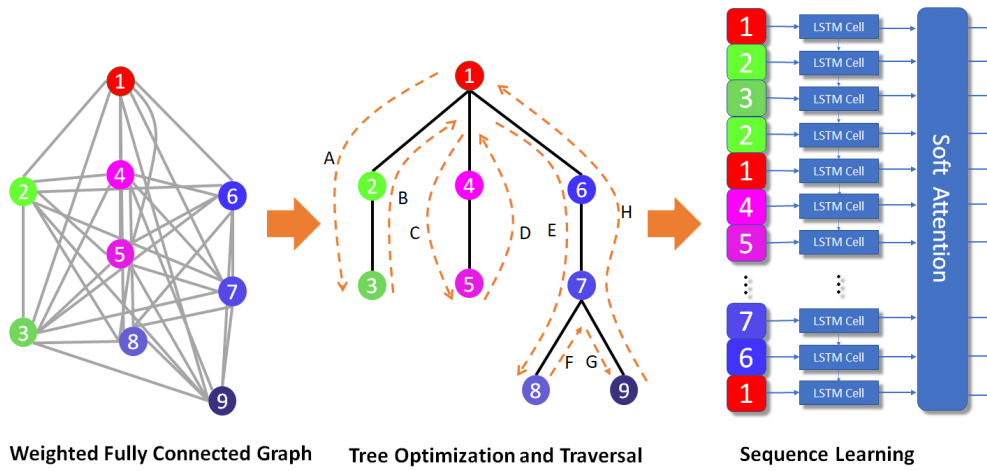


Fig. 3: The details of the tree traversal and the following embedding formation. The built minimum-cost spanning tree is traversed by using Preorder depth first order, which produces the sequence 1-2-3-2-1-4-5-4-1-6-7-8-7-9-7-6-1. The resulting embedding of the sequence is fed to a sequential learner.

the structure stream $H_{structure}$ using:

$$H_{structure} = \sum_i \delta_i h_i. \quad (6)$$

D. Texture Stream

In this stream, the texture information of the input images is used to learn a sequential learner. Like the structure stream, the matrix U determines the input embedding of the sequential learner. Inputs to this stream are the input image I , the matrix λ , and the matrix U . To use the texture information of the input image I , we first create $a \times a$ patches around the center of each facial landmark (the optimal value of parameter a is determined empirically in Section IV-E). The patches are then cropped and fed to a pre-trained encoder, such as ResNet-50 pre-trained on the VGG-Face2 dataset [64].

Suppose that the encoder generates an embedding for the first patch. We call this embedding ψ_1 . We stack the outputs of the encoder for all the patches in a single matrix denoted by $\Psi = [\psi_1 \psi_2 \dots \psi_n]$. By multiplying Ψ and U , we compute the input embedding of the second sequential learner (recall, the first sequential learner was used in the structure stream). Finally, we take the output of this sequential learner from its cells' hidden states and employ an attention mechanism on them similar to the structure stream.

E. Fusion

To combine the outputs of the two attention mechanisms at the end of each of the streams, we employ the fusion strategy proposed in [65] and used in other prior work such as [66]. This fusion strategy was initially created with the goal of preserving the original properties of its input embeddings, and has obtained state-of-the-art results in many areas [65]. We add two dense layers for the output of structure and texture streams. These dense layers act like an encoder to generate stream-specific embeddings. We then employ soft attention to

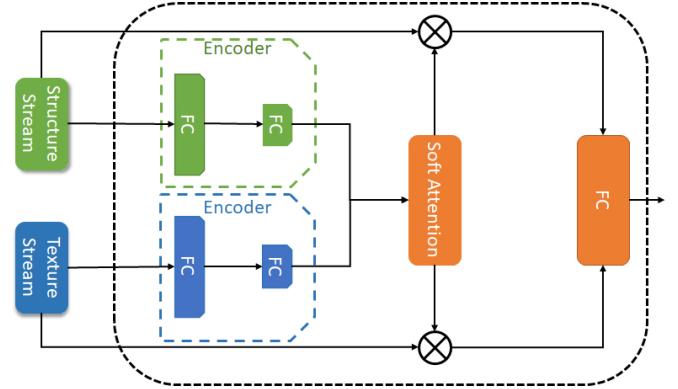


Fig. 4: Illustration of the fusion strategy employed in FaceTopoNet.

learn the weight η using the following equation:

$$\eta = \text{softmax}(\text{tanh}(W_f[T^*, S^*] + b_f)), \quad (7)$$

where W_f and b_f respectively denote the trainable weights and biases, and T^* and S^* respectively denote the stream-specific embeddings from texture and structure streams. Finally, for learning the optimal combination of the two stream-specific embeddings, we utilize a dense layer as:

$$y = \text{tanh}(W_y[(1 + \eta_T)H_{texture}, (1 + \eta_S)H_{structure}] + b_y), \quad (8)$$

where y denotes the final embedding and W_y and b_y represent learnable weights and biases. Finally, y is input to a softmax layer for determining the expression class probability. Figure 4 summarizes the fusion strategy used in this work.

F. Loss Function and Training

Considering each training epoch, a set of weights related to K_n is generated by the CCPSO2 algorithm. These weights are used to form the MST , the traversal of which yields the

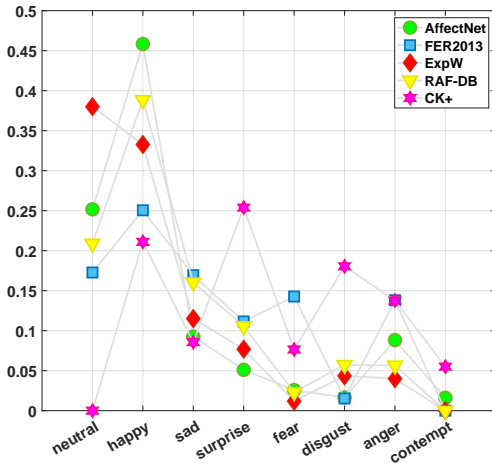


Fig. 5: Distribution of expressions in AffectNet, FER2013, RAF-DB, and ExpW datasets.

matrix U . Next, we freeze the weights of K_n and matrix U and fully train the following texture and structure streams using ADAM optimizer [67]. When the training of the two streams is complete, we feed the final loss value to the CCPSO2 optimization algorithm as its loss function. Given the new loss value, the optimization algorithm creates a set of new weights for the complete graph. This process repeats until convergence.

We define the total loss (\mathcal{L}_{total}) for both CCPSO2 and ADAM optimizers in our end-to-end method as:

$$\mathcal{L}_{total} = \frac{1}{3}(L_1 + L_2 + L_3), \quad (9)$$

where L_1 denotes the fusion loss, and L_2 and L_3 represent the losses for the structure and texture streams respectively. Generally, FER datasets are highly skewed towards a specific expression, usually happy. To demonstrate this, we depict the probability mass function (pmf) of the datasets used in this study (AffectNet, FER2013, RAF-DB, ExpW, and CK+) in Figure 5. This figure clearly demonstrates that the distributions are highly skewed toward Happy class. This issue makes it hard for FER algorithms to perform well on minority classes [68]. To address this issue, we adopt focal loss [69] for all three loss terms in Equation 9. Therefore, the loss terms are defined as:

$$L_i = -\alpha_b(1 - p_b)^\gamma \log(p_b) \quad \text{for } i = 1, 2, 3, \quad (10)$$

where α_b is a balancing factor and p_b is defined by:

$$p_b = \begin{cases} p & y = 1 \\ 1 - p & \text{otherwise,} \end{cases} \quad (11)$$

where y is the ground truth and p is the probability calculated by the model. In Equation 10, γ denotes the focusing parameter. Empirically, we set γ and α_b to 2 and 0.25, respectively. Our use of focal loss allows the model to become less focused on the majority class by down-weighting the samples which are well-classified as shown in the equation.

G. Implementation Details

We implement the proposed architecture using TensorFlow [70] and train it using two Nvidia RTX 2080 Ti GPUs. For ADAM optimizer, we set learning rate, first-momentum decay, and second-momentum-decay as 0.001, 0.9, and 0.99 respectively. For all the experiments, the face images are cropped and resized to $60 \times 60 \times 3$ pixels. Additionally, for data augmentation purpose, each image is horizontally flipped with the probability of 0.25. Similar to [37], [50], [71], the reported results are achieved on the validation set of the respective datasets. However, for CK+ dataset, we use leave-one-subject-out cross validation [72]

Considering CCPSO2 algorithm, the number of iterations is set to 40, as convergence occurs at or before this iteration, after which no changes are observed in the generated trees. Additionally, for random grouping of the variables we use the set $\{1, 5, 7\}$ and the population size for each swarm is set to 10. As CCPSO2 algorithm is a stochastic method, we run it 30 times. However, the converged tree did not change, indicating the consistency of the approach.

IV. EXPERIMENTS

We use four well-known public in-the-wild FER datasets to evaluate our method. In this section, we first introduce these datasets, followed by the details of our experiments, and obtained results.

A. Datasets

AffectNet [25]: Introduced in 2017, AffectNet includes more than 1 million face images. All the images are collected from the Internet using three different search engines. Within the dataset, about 450,000 images have been annotated manually while the remaining have been automatically annotated, i.e. using deep neural networks. Additionally, this dataset provides the ground truth for both the categorical model of affect (happy, sad, surprise, disgust, fear, anger, contempt, and neutral) and the dimensional model of affect, i.e. arousal and valence values for each image. The validation set of AffectNet includes 500 images for each expression class.

FER2013 [26]: Introduced in 2013, FER2013 comprises 28,709 and 7,178 images respectively for training and validation. All the images have the resolution of 48×48 pixels. Moreover, this dataset labels each image in one of the following 6 expression classes: happy, sad, surprise, disgust, fear, anger, and neutral.

RAF-DB [27]: The real-world affective face database (RAF-DB) provides 29,672 face images with their associated expression labels. Crowdsourcing has been used to assign each face image to one of the 7 basic and 11 compound expression classes. Additionally, the dataset has been split into train and validation sets to provide a standard benchmark to the community.

ExpW [28]: This dataset is collected from the Internet by using the Google search engine and offers 91,793 face images. All the images have been labeled manually as one of the 7 basic expression classes.

TABLE I: Obtained recognition rates for different encoders and sequential learners.

Dataset	Encoder	Pretrained on	Sequential Learner			
			LSTM	Bi-LSTM	GRU	Bi-GRU
AffectNet	ResNet-50	VGG-Face2	70.02	69.81	69.91	69.53
	ResNet-50	ImageNet	69.37	68.90	69.23	69.17
	VGG-16	ImageNet	68.21	68.28	68.72	68.42
	BreG-NeXt-50	VGG-Face2	69.43	69.15	69.57	69.43
FER2013	ResNet-50	VGG-Face2	72.66	72.51	72.57	72.43
	ResNet-50	ImageNet	71.26	71.26	71.31	71.23
	VGG-16	ImageNet	71.21	71.19	71.21	71.14
	BreG-NeXt-50	VGG-Face2	72.48	72.37	72.46	72.31
ExpW	ResNet-50	VGG-Face2	71.91	71.83	71.83	71.78
	ResNet-50	ImageNet	70.74	70.66	70.75	70.75
	VGG-16	ImageNet	70.49	70.49	70.54	70.51
RAF-DB	ResNet-50	VGG-Face2	87.80	87.78	87.81	87.74
	ResNet-50	ImageNet	86.93	86.95	87.02	86.87
	VGG-16	ImageNet	86.82	86.77	86.94	86.74
CK+	ResNet-50	VGG-Face2	99.19	98.9	99.19	97.9
	ResNet-50	ImageNet	98.4	97.8	97.3	97.1
	VGG-16	ImageNet	96.3	95.9	96.1	96.3

CK+ [72]: Comprising 327 videos, the extended Cohn-Kanade (CK+) dataset is one of the well-known precursors in the FER datasets. Each video sequence demonstrates a change from neutral to the peak expression. Moreover, CK+ provides the expression labels as being one of the six basic expressions plus contempt expression. For evaluation purpose, we select three peak expression frames within each expression sequence to build train and validation sets.

B. Encoders and Sequential Learners

First we aim to identify the best encoder and sequential learner to be used in FaceTopoNet. Accordingly, we consider several candidates for each sub-module. For the sequential learner we test LSTM, bidirectional LSTM (Bi-LSTM) [80], gated recurrent unit (GRU) [58], and bidirectional GRU (Bi-GRU) [58], while for the encoder, we explore ResNet-50 pre-trained on VGG-Face2, ResNet-50 pre-trained on ImageNet [81], VGG-16 pre-trained on ImageNet, and BreG-NeXt-50 pretrained on VGG-Face2 for encoder. These sub-modules have been selected for experimentation given their strong performance in prior work [50], [82]. We report the FER results for each dataset in Table I. Given the results, the best combination for 4 of the datasets is achieved with a ResNet-50 pretrained on VGG-Face2 and LSTM. The only exception is on the RAF-DB dataset in which GRU exhibits slightly (marginal) better performance than the LSTM. Additionally, regarding CK+, GRU-ResNet-50 combination delivers the same accuracy as the LSTM-ResNet-50 combination. Hence, for the sake of consistency in our experiments, we use a ResNet-50 and LSTM in FaceTopoNet. We observe from the table that pre-training on VGG-Face2 obtains better results compared to ImageNet, which is predictable given that VGG-Face2 only includes face images with different poses and illuminations as opposed to ImageNet which contains various image classes of different objects. This can help the encoder to extract embeddings that are discriminative and important in the context of human faces. Moreover, we observe that the added depth and residual connections of ResNet-50 results in better performance compared to VGG-16.

C. Performance

We report the RR values for FaceTopoNet along with other state-of-the-art benchmarks on all 5 datasets in Tables II through VI. Considering AffectNet (Table II), FaceTopoNet outperforms the state-of-the-art FER methods BreG-NeXt-50 and BreGNeXt-32 by 1.52% and 3.28%, respectively. With regards to FER2013 dataset (Table III), FaceTopoNet shows an improvement of 1.13% over the state-of-the-art, BreG-NeXt-50. The results for ExpW are presented in Table V. In this table, we can observe that FaceTopoNet has the highest recognition rate (71.91%) compared to other methods. This is followed by [83], which also uses part-based methods, dividing the face into different sections, to perform FER. The results for RAF-DB are presented in Table IV. As it is evident from this table, our method achieves the second-best recognition rate, being marginally below [84] by only 0.27%. A reason for this could be the use of a new loss term by [84], which is equipped to handle class imbalances, which is a common issue in FER datasets, by monitoring the last layers of a CNN. Finally, regarding CK+ dataset, FaceTopoNet achieves the second best recognition rate. The current state-of-the-art [42] offers the recognition rate of 99.54%, while FaceTopoNet achieves slightly lower recognition rate, 99.19%.

As some of the state-of-the-art methods additionally reported precision and recall values for both AffectNet and FER2013 datasets, we also consider these measures for each emotion class in Tables II and III. As it is evident from Table II, for most of the expression classes, FaceTopoNet outperforms other state-of-the-art methods in terms of precision and recall. More specifically, FaceTopoNet obtains the best precision and recall in disgust and contempt expressions, which are considered as more difficult classes due to their small numbers of training samples in the AffectNet dataset. Given FER2013 dataset, FaceTopoNet delivers the highest precision in most of the expression classes - i.e. neutral, sad, fear, and angry - while achieving the state-of-the-art recall in 3 expression classes.

For a deeper comparison between our proposed model and one of the best performing benchmarks in both AffectNet and FER2013 datasets, BreG-NeXt-50, F1 scores corresponding to

TABLE II: Results of FaceTopoNet on AffectNet dataset. ‘Ne.’, ‘Ha.’, ‘Sa.’ ‘Su.’, ‘Fe.’, ‘Di.’, ‘An.’, and ‘Co.’, denote neutral, happy, sad, surprise, fear, disgust, anger, and contempt respectively.

Authors	Method	RR	Precision								Recall							
			Ne.	Ha.	Sa.	Su.	Fe.	Di.	An.	Co.	Ne.	Ha.	Sa.	Su.	Fe.	Di.	An.	Co.
Hewitt et al. [73]	CNN	58	45	76	59	55	60	55	57	59	49	72	56	60	64	63	43	56
Hua et al. [74]	Ensemble	62.11	58	72	64	62	57	59	62	-	59	70	67	66	61	59	57	
Hasani et al. [50]	BreG-NeXt32	66.74																
Hasani et al. [50]	BreG-NeXt50	68.50	72	78	62	66	67	62	63	67	53	89	66	74	63	77	61	58
Chen et al. [75]	Residual multi-task learning	61.98																
Zhang et al. [76]	Pseudo-siamese structure	63.70																
Farzaneh et al. [77]	Deep attentive center loss	65.20																
Ours	FaceTopoNet	70.02	72	63	75	65	68	72	74	77	38	98	66	78	63	88	68	59

TABLE III: Results of FaceTopoNet on FER2013 dataset.

Authors	Method	RR	Precision							Recall								
			Ne.	Ha.	Sa.	Su.	Fe.	Di.	An.	Ne.	Ha.	Sa.	Su.	Fe.	Di.	An.		
Vielzeuf et al. [71]	CNN	71.2																
Hasani et al. [50]	BreG-NeXt32	69.11																
Hasani et al. [50]	BreG-NeXt50	71.53	69	88	59	78	52	62	60	69	90	62	80	46	12	65		
Shi et al. [78]	cross-connected CNN	71.52																
Pourramezan et al. [79]	Deep metric learning	72.03	63	90	61	80	61	75	63	73	88	56	83	59	77	62		
Ours	FaceTopoNet	72.66	71	63	63	70	63	42	66	64	93	64	82	54	20	73		

TABLE IV: Results of FaceTopoNet on RAF-DB dataset

Author	Method	RR
Wang et al. [86]	pseudo-siamese network	86.50
Wang et al. [35]	Region attention	86.90
Wang et al. [87]	Attention and relabeling	87.03
Farzaneh et al. [77]	CNN and attention	87.78
Li et al. [84]	Coarse-fine labeling	88.07
Ours	FaceTopoNet	87.80

TABLE VI: Results of FaceTopoNet on CK+ dataset

Author	Method	RR
Ruan et al. [42]	Feature decomposition and reconstruction	99.54
Ruan et al. [90]	removal of disturbing factors	99.16
Yang et al. [91]	De-expression residue learning	97.30
Zeng et al. [92]	Latent truth net	92.45
Liu et al. [93]	combining the deep metric and softmax loss	97.10
Ours	FaceTopoNet	99.19

TABLE V: Results of FaceTopoNet on ExpW dataset.

Author	Method	RR
Benamaraet et al. [88]	Ensemble	71.82
Xie et al. [18]	Adversarial graph representation	68.50
Lain et al. [83]	CNN-Prediction authenticity	71.90
Peng et al. [89]	Domain adaptive FER	70.86
Ours	FaceTopoNet	71.91

the expression classes are presented in Figure 6 using one-vs-all method [85]. Considering AffectNet, our proposed method obtains higher F1 scores in 6 out of 8 expressions when compared to BreG-NeXt-50, while in FER2013 we outperform BreG-NeXt-50 in 4 of the 7 classes.

We depict the obtained confusion matrices between the ground truth and the predicted expressions using our proposed method in Figure 7. For AffectNet, 3 cases, including contempt-happy, sad-surprise, and neutral-happy (the first and second elements are respectively the ground truth and the predicted expression) have the largest confusions. Confusion between contempt and happy is prevalent and expected in FER systems given the high semantic similarity of the two classes, and as evidenced by high confusion rates obtained from the perspective of human observers [50]. Regarding FER2013, disgust-happy has the largest confusion. This is due to the fact that happy and disgust are respectively the majority and minority expression classes within the dataset causing a bias within the model (see the pmf for FER2013 in Figure 5). Despite the fact that we adopt focal loss to address the issue of the imbalanced training set, FaceTopoNet still identifies

some of the disgust cases (minority class) as happy (majority class). Apart from disgust, FaceTopoNet performs well on the FER2013 dataset overall. On the RAF-DB dataset, the largest confusions occur in the case of disgust-sad as well as disgust-neutral. The same issue can be seen in some of the prior works on RAF-DB [94]. As for the ExpW dataset, fear is confused with neutral, happy, and sad expressions. This can be justified as fear only constitutes 1.1% of the ExpW dataset. Finally, considering CK+ dataset, happy and disgust expressions have the highest accuracy. Additionally, the largest confusions occur in contempt-fear and sad-disgust cases. Among the expressions within the CK+, disgust expression shows the lowest error, while fear shows the highest error.

The key concept behind the good performance of our method is the “ordering” of the embeddings. In Figure 1, we have demonstrated that the ordering of the embeddings can affect the performance of sequential learners. Thus, our model optimizes the ordering of the embeddings, such that it becomes easy for a sequential learner to model the dependencies which exists among these embeddings. In this way, the sequential learner delivers superior performance.

D. Optimal Number of Extracted Facial Landmarks

To choose the optimal value of the parameter n (number of the extracted facial landmarks), we increase it by 10 each time and report the performance. The resulting curve is shown in Figure 8 for both AffectNet and FER2013 datasets. Considering AffectNet dataset, there is a direct relationship

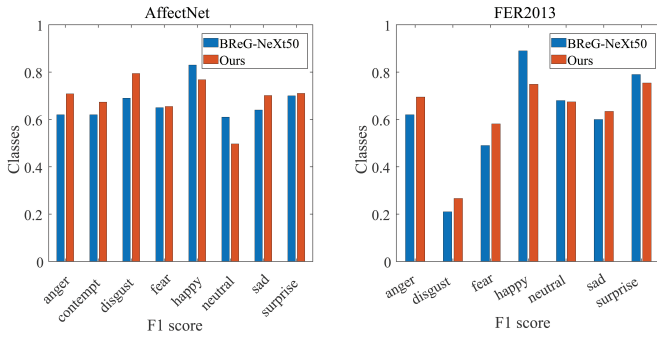


Fig. 6: Achieved F1 scores of BreG-NeXt50 and FaceTopoNet.

between n and the performance, up until 50 facial landmarks, from where the performance starts to drop. This behaviour can be justified as the n increases, the overlap between the patches around these landmarks, and thus the redundant information increases. Almost the same behaviour can be seen for the FER2013 dataset. To be consistent in all the experiments, we set the value of n as 50.

E. Optimal Patch Size

As mentioned earlier in III-D, we apply $a \times a$ patches over each of the extracted facial landmarks, and subsequently feed these patches to the encoder to extract texture information. In this experiment, we aim to find the optimal value for the parameter a . To this end, we first consider 4×4 patches for training FaceTopoNet on both AffectNet and FER2013 datasets. Next, we repeat the experiment by increasing a by 1. We continue this process until no performance increase is observed. Figure 9 depicts the changes in RR with respect to the changes in a for both datasets. This figure shows that the highest RR for AffectNet and FER2013 occurs at $a = 17$ and $a = 16$ respectively. The small difference between the optimal patch sizes of the two datasets indicates low dependency of a on the dataset. For consistency, we set $a = 17$ throughout our experimental setup.

F. Robustness Occlusion

Here, we evaluate the robustness of FaceTopoNet and the state-of-the-art BreG-NeXt-50 against synthetic occlusions placed on key areas of the face. Considering the availability of the state-of-the-art pre-trained models on AffectNet and FER2013, we decide to perform this experiment on these two datasets. To this end, we extract the key components of face images, namely two eyes, mouth, and nose, using OpenCV [95] and dlib [96] libraries. We then add black patches on these key areas, and subsequently build three new validation sets for each of the AffectNet and FER2013 datasets to test our model against. We name these validation sets “eye-removed”, “mouth-removed”, and “nose-removed”. Figure 10 shows a sample image along with the associated occlusions. The performance of our model on both datasets is shown in Figure 11, where FaceTopoNet delivers better RRs (0.6% average gain) compared to Breg-NeXt-50 in all the occlusion scenarios. This demonstrates the robustness of our

TABLE VII: Cross-dataset study

Dataset	Tree	RR
AffectNet	FER2013	68.48
FER2013	AffectNet	71.40
AffectNet	Human-designed [20]	65.91
FER2013	Human-designed [20]	67.26

method against the considered occlusions. Additionally, this experiment reveals that mouth and eyes have approximately the same contribution in expression recognition, since “eye-removed” and “mouth-removed” scenarios show roughly the same RR drop. This finding is in line with previous studies such as [97].

G. Tree Topology Evolution

The evolution of the topology of the face trees in the training phase of FaceTopoNet can provide some additional insights into the learning process. Figure 12 depicts the topological evolution of the minimum-cost spanning trees generated by FaceTopoNet in iterations 1 and 40 for AffectNet, FER2013, RAF-DB, and ExpW datasets. In the beginning of the training phase, as the weights of K_n are random, the trees are also random. However, as the training progresses, the face trees become more resembling of the structure of a human face. Moreover, from the face trees created in iteration 40, it is evident that there exists variations between the face tree created for each dataset, particularly around nose and mouth regions. This is not unexpected given the importance of these regions in FER.

H. Cross-Dataset Study and Comparison to Human-Designed Face Tree

Here, we aim to explore *whether or not the trees generated by FaceTopoNet can be used in transfer learning*. To this end, we perform a cross-dataset study by using the final tree originally learned using AffectNet for expression recognition on the FER2013 dataset, and vice-versa. Table VII presents the results where we observe an RR drop of 1.54% and 1.26% for AffectNet and FER2013 datasets, respectively. From this experiment, we conclude that while the learned trees are customized and optimized for individual datasets, given the similarities between the datasets, it is reasonably feasible to perform cross-dataset tree-based transfer learning.

Next we compare the trees generated by FaceTopoNet with human-designed trees which have been used in other literature [20] (see Figure 12 (b)). This tree is built based on the physiological as and psychological properties of human faces. Thus, we use this tree to perform FER on AffectNet and FER2013 datasets instead of using the customized trees learned for each individual dataset. Table VII illustrates the results where we observe a drop of 4.11% and 5.4% for AffectNet and FER2013 datasets, respectively. We can therefore infer that FaceTopoNet-generated trees are more optimized for conducting FER for various datasets in comparison to human-designed trees.

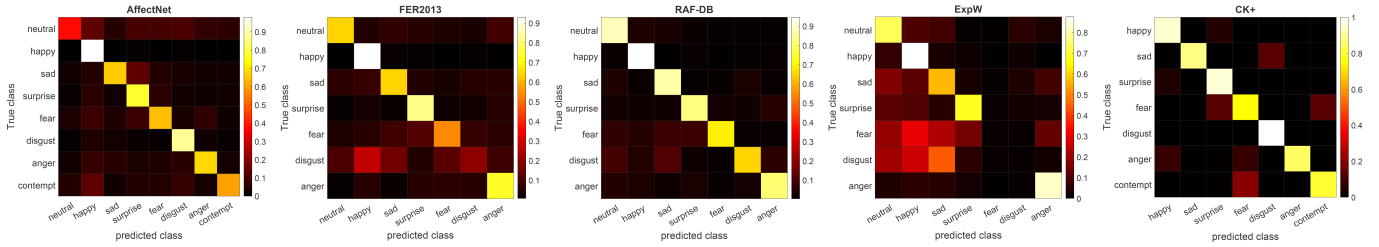


Fig. 7: FaceTopoNet’s Confusion Matrices.

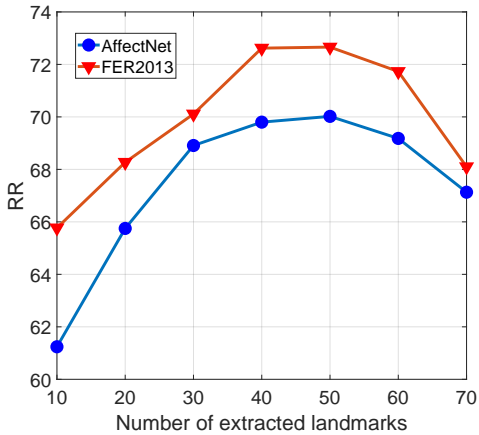


Fig. 8: Changes in RR with the changes in the number of extracted landmarks

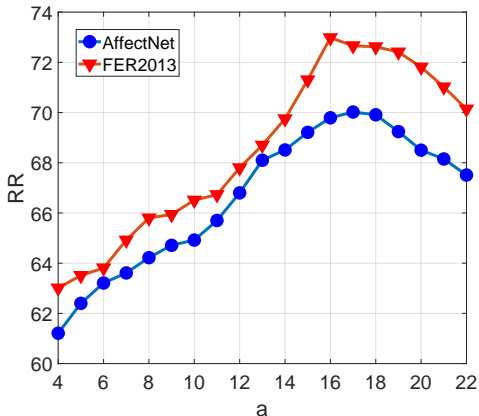


Fig. 9: Changes in RR with the changes in a .

I. Ablation study

We conduct ablation experiments to evaluate the contribution of different components of our pipeline. This is done by systematic removal of the components of FaceTopoNet and calculating the resulting drop in performance. We present the results of this study in Table VIII, where (i) the tree topology learning step is removed and replaced by a random tree since the model requires a tree; (ii) the texture stream is removed; (iii) the structure stream is removed; and (iv) the final fusion step is removed and replaced by a simple concatenation. From the results outlined in Table VIII, we observe that the removal of the tree topology learning step

TABLE VIII: Ablation study. Recognition rates (RR) and the resulting drop in RR are provided when a specific component is removed from FaceTopoNet

Removed	RR		Drop in RR	
	AffectNet	FER2013	AffectNet	FER2013
Tree topology	66.51%	67.11%	5.0%	7.60%
Structure stream	64.90%	66.02%	7.30%	9.14%
Texture stream	62.14%	63.17%	11.25%	13.06%
Fusion strategy	66.87%	68.24%	4.50%	6.08%

TABLE IX: Inference time of different methods

Author	Method	Inference time (ms)
Wang et al. [35]	Region attention	24
Kuo et al. [98]	Compact CNN	21
Ours	FaceTopoNet	33

results in substantial performance drop of 5.0% and 7.60%, respectively for AffectNet and FER2013 datasets. Moreover, it is shown that while both texture and structure streams are critical toward the final performance, the texture stream plays a more critical role. This can be attributed to the higher richness of information in texture patches versus structure coordinates. Lastly the model also exhibits a drop in performance when the two-stream fusion strategy is replaced with a simple feature-level fusion, revealing the importance of conducting a proper fusion in the final step of FaceTopoNet.

J. Limitations

We perform an experiment to estimate the inference time of our method and compare it with that of prior work. To this end, we apply FaceTopoNet over 100 test images and average the corresponding inference time. Also, we find [35] and [98] which report their inference time in the context of FER. For a fair comparison, we re-run their method on our local machine with the same hardware used to record the inference time of FaceTopoNet. From Table IX, it is evident that FaceTopoNet’s run-time is higher, but only by a small margin. One of the ways by which FaceTopoNet can be improved is using faster algorithms for the calculation of the minimum-cost spanning tree.

V. CONCLUSION

In this paper, we present a new end-to-end deep pipeline, termed FaceTopoNet, for learning the topology of face graphs for facial expression recognition systems. FaceTopoNet first

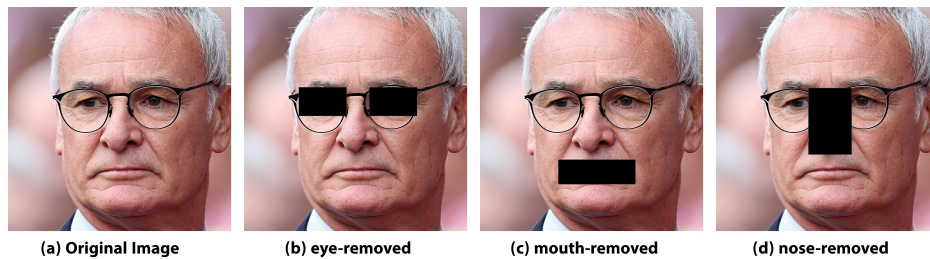


Fig. 10: Added occlusions on an image from AffectNet dataset

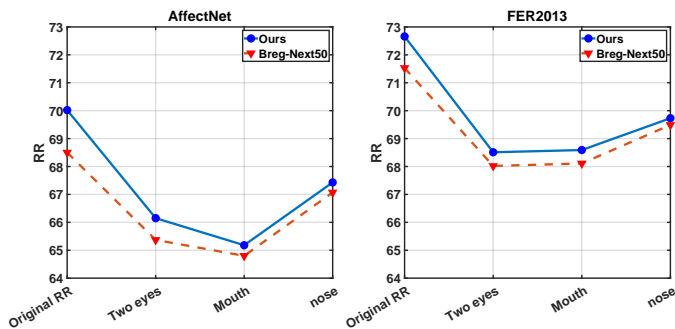


Fig. 11: Changes of RR with regards to different types of occlusions

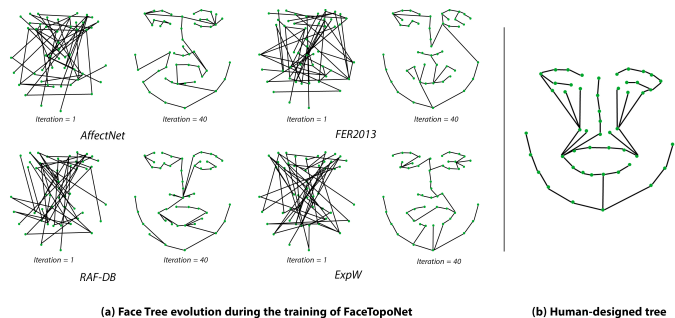


Fig. 12: Face trees obtained by FaceTopoNet and Human-designed face tree borrowed from [20]

extracts facial landmarks which are then used to create a fully connected graph. The weights of the graph are then optimized to create a minimum-cost spanning tree, which is then traversed to create a sequence. This sequence is subsequently used to design the input embeddings of two sequential learners in two parallel streams within our model. The first stream relies on the coordinates of the landmarks to learn the structure of the face, while the second stream learns texture information using patches around each extracted landmark. The outputs of each stream are then passed through an attention mechanism to focus on more salient features, prior to being fused. We perform extensive experiments on 4 popular in-the-wild FER datasets, AffectNet, FER2013, RAF-DB, and ExpW. Results indicate that not only FaceTopoNet sets new state-of-the-art recognition rate in AffectNet, FER2013, and ExpW datasets, but also shows more robustness against different occlusions. We also perform detailed ablation and sensitivity studies to

study our model in depth.

Future work may include using new optimization approaches such as reinforcement learning for further optimization of the tree structure. Moreover, our approach may be used for optimization of the structure of graph convolutional neural networks used for face representation learning.

REFERENCES

- [1] N. Jaques, D. McDuff, Y. L. Kim, and R. Picard, "Understanding and predicting bonding in conversations using thin slices of facial expressions and body language," in *International Conference on Intelligent Virtual Agents*. Springer, 2016, pp. 64–74.
- [2] R. W. Picard, *Affective computing*. MIT press, 2000.
- [3] A. Sepas-Moghaddam, A. Etemad, F. Pereira, and P. L. Correia, "Capsfield: light field-based face and expression recognition in the wild using capsule routing," *arXiv preprint arXiv:2101.03503*, 2021.
- [4] R. Shuvendu and A. Etemad, "Self-supervised contrastive learning of multi-view facial expressions," in *Proceedings of the 2021 International Conference on Multimodal Interaction*, 2021.
- [5] A. Sepas-Moghaddam, A. Etemad, F. Pereira, and P. L. Correia, "Facial emotion recognition using light field images with deep attention-based bidirectional lstm," in *ICASSP 2020-2020 IEEE International Conference on Acoustics, Speech and Signal Processing (ICASSP)*. IEEE, 2020, pp. 3367–3371.
- [6] A. Sepas-Moghaddam, A. Etemad, P. L. Correia, and F. Pereira, "A deep framework for facial emotion recognition using light field images," in *2019 8th International Conference on Affective Computing and Intelligent Interaction (ACII)*. IEEE, 2019, pp. 1–7.
- [7] G. Bargshady, X. Zhou, R. C. Deo, J. Soar, F. Whittaker, and H. Wang, "Enhanced deep learning algorithm development to detect pain intensity from facial expression images," *Expert Systems with Applications*, vol. 149, p. 113305, 2020.
- [8] W. Pei, H. Dibeklioğlu, T. Baltrušaitis, and D. M. Tax, "Attended end-to-end architecture for age estimation from facial expression videos," *IEEE Transactions on Image Processing*, vol. 29, pp. 1972–1984, 2019.
- [9] S. Porcu, A. Floris, J.-N. Voigt-Antons, L. Atzori, and S. Möller, "Estimation of the quality of experience during video streaming from facial expression and gaze direction," *IEEE Transactions on Network and Service Management*, vol. 17, no. 4, pp. 2702–2716, 2020.
- [10] X. Li, W. Guo, and H. Yang, "Depression severity prediction from facial expression based on the drr_depressionnet network," in *2020 IEEE International Conference on Bioinformatics and Biomedicine (BIBM)*. IEEE, 2020, pp. 2757–2764.
- [11] S. Li and W. Deng, "Deep facial expression recognition: A survey," *IEEE Transactions on Affective Computing*, vol. 13, no. 3, pp. 1195–1215, 2022.
- [12] H. Jung, S. Lee, J. Yim, S. Park, and J. Kim, "Joint fine-tuning in deep neural networks for facial expression recognition," in *Proceedings of the IEEE international conference on computer vision*, 2015, pp. 2983–2991.
- [13] D. Ghimire, S. Jeong, J. Lee, and S. H. Park, "Facial expression recognition based on local region specific features and support vector machines," *Multimedia Tools and Applications*, vol. 76, no. 6, pp. 7803–7821, 2017.
- [14] S. Happy, A. Dantcheva, and F. Bremond, "Expression recognition with deep features extracted from holistic and part-based models," *Image and Vision Computing*, p. 104038, 2020.

- [15] X. Liu, B. V. Kumar, P. Jia, and J. You, "Hard negative generation for identity-disentangled facial expression recognition," *Pattern Recognition*, vol. 88, pp. 1–12, 2019.
- [16] M. Yu, H. Zheng, Z. Peng, J. Dong, and H. Du, "Facial expression recognition based on a multi-task global-local network," *Pattern Recognition Letters*, vol. 131, pp. 166–171, 2020.
- [17] H.-X. Xie, L. Lo, H.-H. Shuai, and W.-H. Cheng, "Au-assisted graph attention convolutional network for micro-expression recognition," in *ACM International Conference on Multimedia*, 2020, pp. 2871–2880.
- [18] Y. Xie, T. Chen, T. Pu, H. Wu, and L. Lin, "Adversarial graph representation adaptation for cross-domain facial expression recognition," in *ACM International Conference on Multimedia*, 2020, pp. 1255–1264.
- [19] L. Zhong, C. Bai, J. Li, T. Chen, S. Li, and Y. Liu, "A graph-structured representation with brnn for static-based facial expression recognition," in *IEEE International Conference on Automatic Face & Gesture Recognition*, 2019, pp. 1–5.
- [20] J. Zhou, X. Zhang, Y. Liu, and X. Lan, "Facial expression recognition using spatial-temporal semantic graph network," in *2020 IEEE International Conference on Image Processing (ICIP)*. IEEE, 2020, pp. 1961–1965.
- [21] L. Lei, J. Li, T. Chen, and S. Li, "A novel graph-tcn with a graph structured representation for micro-expression recognition," in *ACM International Conference on Multimedia*, 2020, pp. 2237–2245.
- [22] X. Xu, Z. Ruan, and L. Yang, "Facial expression recognition based on graph neural network," in *International Conference on Image, Vision and Computing*, 2020, pp. 211–214.
- [23] Y. Liu, X. Zhang, Y. Lin, and H. Wang, "Facial expression recognition via deep action units graph network based on psychological mechanism," *IEEE Transactions on Cognitive and Developmental Systems*, vol. 12, no. 2, pp. 311–322, 2019.
- [24] X. Li and X. Yao, "Cooperatively coevolving particle swarms for large scale optimization," *IEEE Transactions on Evolutionary Computation*, vol. 16, no. 2, pp. 210–224, 2011.
- [25] A. Mollahosseini, B. Hasani, and M. H. Mahoor, "Affectnet: A database for facial expression, valence, and arousal computing in the wild," *IEEE Transactions on Affective Computing*, vol. 10, no. 1, pp. 18–31, 2017.
- [26] I. J. Goodfellow, D. Erhan, P. L. Carrier, A. Courville, M. Mirza, B. Hamner, W. Cukierski, Y. Tang, D. Thaler, D.-H. Lee *et al.*, "Challenges in representation learning: A report on three machine learning contests," in *International Conference on Neural Information Processing*, 2013, pp. 117–124.
- [27] S. Li, W. Deng, and J. Du, "Reliable crowdsourcing and deep locality-preserving learning for expression recognition in the wild," in *2017 IEEE Conference on Computer Vision and Pattern Recognition (CVPR)*. IEEE, 2017, pp. 2584–2593.
- [28] Z. Zhang, P. Luo, C. C. Loy, and X. Tang, "From facial expression recognition to interpersonal relation prediction," in *arXiv:1609.06426v2*, September 2016.
- [29] M. Kolahdouzi, A. Sepas-Moghaddam, and A. Etemad, "Face trees for expression recognition," in *2021 16th IEEE International Conference on Automatic Face and Gesture Recognition (FG 2021)*, 2021, pp. 1–5.
- [30] Y. Tang, "Deep learning using linear support vector machines," *arXiv preprint arXiv:1306.0239*, 2013.
- [31] A. Yao, D. Cai, P. Hu, S. Wang, L. Sha, and Y. Chen, "Holonet: towards robust emotion recognition in the wild," in *Proceedings of the 18th ACM International Conference on Multimodal Interaction*, 2016, pp. 472–478.
- [32] W. Shang, K. Sohn, D. Almeida, and H. Lee, "Understanding and improving convolutional neural networks via concatenated rectified linear units," in *International Conference on Machine Learning*, 2016, pp. 2217–2225.
- [33] D. V. Sang, N. Van Dat *et al.*, "Facial expression recognition using deep convolutional neural networks," in *International Conference on Knowledge and Systems Engineering*, 2017, pp. 130–135.
- [34] Y. Chen, J. Wang, S. Chen, Z. Shi, and J. Cai, "Facial motion prior networks for facial expression recognition," in *IEEE Visual Communications and Image Processing*, 2019.
- [35] K. Wang, X. Peng, J. Yang, D. Meng, and Y. Qiao, "Region attention networks for pose and occlusion robust facial expression recognition," *IEEE Transactions on Image Processing*, vol. 29, pp. 4057–4069, 2020.
- [36] P. Jiang, G. Liu, Q. Wang, and J. Wu, "Accurate and reliable facial expression recognition using advanced softmax loss with fixed weights," *IEEE Signal Processing Letters*, vol. 27, pp. 725–729, 2020.
- [37] D. Kollias, S. Cheng, E. Ververas, I. Kotsia, and S. Zafeiriou, "Deep neural network augmentation: Generating faces for affect analysis," *International Journal of Computer Vision*, pp. 1–30, 2020.
- [38] J. Booth, E. Antonakos, S. Ploumpis, G. Trigeorgis, Y. Panagakis, and S. Zafeiriou, "3d face morphable models" in-the-wild," in *Proceedings of the IEEE Conference on Computer Vision and Pattern Recognition*, 2017, pp. 48–57.
- [39] Z. Zhao, Q. Liu, and S. Wang, "Learning deep global multi-scale and local attention features for facial expression recognition in the wild," *IEEE Transactions on Image Processing*, vol. 30, pp. 6544–6556, 2021.
- [40] F. Xue, Q. Wang, and G. Guo, "Transfer: Learning relation-aware facial expression representations with transformers," in *Proceedings of the IEEE/CVF International Conference on Computer Vision*, 2021, pp. 3601–3610.
- [41] J. Cai, Z. Meng, A. S. Khan, J. O'Reilly, Z. Li, S. Han, and Y. Tong, "Identity-free facial expression recognition using conditional generative adversarial network," in *2021 IEEE International Conference on Image Processing (ICIP)*. IEEE, 2021, pp. 1344–1348.
- [42] D. Ruan, Y. Yan, S. Lai, Z. Chai, C. Shen, and H. Wang, "Feature decomposition and reconstruction learning for effective facial expression recognition," in *Proceedings of the IEEE/CVF Conference on Computer Vision and Pattern Recognition*, 2021, pp. 7660–7669.
- [43] W. Huang, S. Zhang, P. Zhang, Y. Zha, Y. Fang, and Y. Zhang, "Identity-aware facial expression recognition via deep metric learning based on synthesized images," *IEEE Transactions on Multimedia*, 2021.
- [44] Y. Choi, M. Choi, M. Kim, J.-W. Ha, S. Kim, and J. Choo, "Stargan: Unified generative adversarial networks for multi-domain image-to-image translation," in *Proceedings of the IEEE conference on computer vision and pattern recognition*, 2018, pp. 8789–8797.
- [45] C. Bisogni, A. Castiglione, S. Hossain, F. Narducci, and S. Umer, "Impact of deep learning approaches on facial expression recognition in healthcare industries," *IEEE Transactions on Industrial Informatics*, vol. 18, no. 8, pp. 5619–5627, 2022.
- [46] S. Hossain, S. Umer, V. Asari, and R. K. Rout, "A unified framework of deep learning-based facial expression recognition system for diversified applications," *Applied Sciences*, vol. 11, no. 19, p. 9174, 2021.
- [47] S. Umer, R. K. Rout, C. Pero, and M. Nappi, "Facial expression recognition with trade-offs between data augmentation and deep learning features," *Journal of Ambient Intelligence and Humanized Computing*, vol. 13, no. 2, pp. 721–735, 2022.
- [48] I. Oztel, G. Yolcu, C. Öz, S. Kazan, and F. Bunyak, "ifer: facial expression recognition using automatically selected geometric eye and eyebrow features," *Journal of Electronic Imaging*, vol. 27, no. 2, p. 023003, 2018.
- [49] B. Hasani, P. S. Negi, and M. H. Mahoor, "Bounded residual gradient networks (breg-net) for facial affect computing," in *2019 14th IEEE International Conference on Automatic Face & Gesture Recognition (FG 2019)*. IEEE, 2019, pp. 1–7.
- [50] B. Hasani, P. S. Negi, and M. Mahoor, "Breg-next: facial affect computing using adaptive residual networks with bounded gradient," *IEEE Transactions on Affective Computing*, vol. 13, no. 2, p. 1, 2022.
- [51] D. Teney, L. Liu, and A. van Den Hengel, "Graph-structured representations for visual question answering," in *Proceedings of the IEEE Conference on Computer Vision and Pattern Recognition*, 2017, pp. 1–9.
- [52] Y. Li, D. Tarlow, M. Brockschmidt, and R. Zemel, "Gated graph sequence neural networks," *arXiv preprint arXiv:1511.05493*, 2015.
- [53] P. Antoniadis, P. P. Filintisis, and P. Maragos, "Exploiting emotional dependencies with graph convolutional networks for facial expression recognition," *arXiv preprint arXiv:2106.03487*, 2021.
- [54] D. Liu, H. Zhang, and P. Zhou, "Video-based facial expression recognition using graph convolutional networks," in *2020 25th International Conference on Pattern Recognition (ICPR)*. IEEE, 2021, pp. 607–614.
- [55] J. Zhou, X. Zhang, Y. Liu, and X. Lan, "Facial expression recognition using spatial-temporal semantic graph network," in *2020 IEEE International Conference on Image Processing (ICIP)*. IEEE, 2020, pp. 1961–1965.
- [56] M. Liu, S. Li, S. Shan, R. Wang, and X. Chen, "Deeply learning deformable facial action parts model for dynamic expression analysis," in *Asian Conference on Computer Vision*. Springer, 2014, pp. 143–157.
- [57] D. Liu, H. Zhang, and P. Zhou, "Video-based facial expression recognition using graph convolutional networks," *arXiv preprint arXiv:2010.13386*, 2020.
- [58] K. Cho, B. Van Merriënboer, C. Gulcehre, D. Bahdanau, F. Bougares, H. Schwenk, and Y. Bengio, "Learning phrase representations using rnn encoder-decoder for statistical machine translation," *arXiv preprint arXiv:1406.1078*, 2014.
- [59] J. Lv, X. Shao, J. Xing, C. Cheng, and X. Zhou, "A deep regression architecture with two-stage re-initialization for high performance facial landmark detection," in *Proceedings of the IEEE Conference on Computer Vision and Pattern Recognition*, 2017, pp. 3317–3326.

- [60] B. Jiang and L. Zhang, "Research on minimum spanning tree based on prim algorithm," *Computer Engineering and Design*, vol. 13, 2009.
- [61] D. C. Kozen, "Depth-first and breadth-first search," in *The Design and Analysis of Algorithms*. Springer, 1992, pp. 19–24.
- [62] F. A. Gers and J. Schmidhuber, "Recurrent nets that time and count," in *Proceedings of the IEEE-INNS-ENNS International Joint Conference on Neural Networks. IJCNN 2000. Neural Computing: New Challenges and Perspectives for the New Millennium*, vol. 3. IEEE, 2000, pp. 189–194.
- [63] T. Rocktäschel, E. Grefenstette, K. M. Hermann, T. Kočiský, and P. Blunsom, "Reasoning about entailment with neural attention," *arXiv preprint arXiv:1509.06664*, 2015.
- [64] Q. Cao, L. Shen, W. Xie, O. M. Parkhi, and A. Zisserman, "Vggface2: A dataset for recognising faces across pose and age," in *2018 13th IEEE International Conference on Automatic Face & Gesture Recognition (FG 2018)*. IEEE, 2018, pp. 67–74.
- [65] Y. Gu, K. Yang, S. Fu, S. Chen, X. Li, and I. Marsic, "Hybrid attention based multimodal network for spoken language classification," in *Proceedings of the Conference. Association for Computational Linguistics Meeting*, vol. 2018. NIH Public Access, 2018, p. 2379.
- [66] G. Zhang and A. Etamad, "Rfnet: riemannian fusion network for eeg-based brain-computer interfaces," *arXiv preprint arXiv:2008.08633*, 2020.
- [67] D. P. Kingma and J. Ba, "Adam: a method for stochastic optimization. arxiv," *arXiv preprint arXiv:1412.6980*, vol. 22, 2014.
- [68] H. He and E. A. Garcia, "Learning from imbalanced data," *IEEE Transactions on Knowledge and Data Engineering*, vol. 21, no. 9, pp. 1263–1284, 2009.
- [69] T.-Y. Lin, P. Goyal, R. Girshick, K. He, and P. Dollár, "Focal loss for dense object detection," in *Proceedings of the IEEE International Conference on Computer Vision*, 2017, pp. 2980–2988.
- [70] M. Abadi, P. Barham, J. Chen, Z. Chen, A. Davis, J. Dean, M. Devin, S. Ghemawat, G. Irving, M. Isard *et al.*, "Tensorflow: A system for large-scale machine learning," in *12th {USENIX} Symposium on Operating Systems Design and Implementation ({OSDI} 16)*, 2016, pp. 265–283.
- [71] V. Vielzeuf, S. Pateux, and F. Jurie, "Temporal multimodal fusion for video emotion classification in the wild," in *Proceedings of the 19th ACM International Conference on Multimodal Interaction*, 2017, pp. 569–576.
- [72] P. Lucey, J. F. Cohn, T. Kanade, J. Saragih, Z. Ambadar, and I. Matthews, "The extended cohn-kanade dataset (ck+): A complete dataset for action unit and emotion-specified expression," in *2010 IEEE Computer Society Conference on Computer Vision and Pattern Recognition-Workshops*. IEEE, 2010, pp. 94–101.
- [73] C. Hewitt and H. Gunes, "Cnn-based facial affect analysis on mobile devices," *arXiv preprint arXiv:1807.08775*, 2018.
- [74] W. Hua, F. Dai, L. Huang, J. Xiong, and G. Gui, "Hero: Human emotions recognition for realizing intelligent internet of things," *IEEE Access*, vol. 7, pp. 24 321–24 332, 2019.
- [75] B. Chen, W. Guan, P. Li, N. Ikeda, K. Hirasawa, and H. Lu, "Residual multi-task learning for facial landmark localization and expression recognition," *Pattern Recognition*, vol. 115, p. 107893, 2021.
- [76] W. Zhang, X. Ji, K. Chen, Y. Ding, and C. Fan, "Learning a facial expression embedding disentangled from identity," in *Proceedings of the IEEE/CVF Conference on Computer Vision and Pattern Recognition*, 2021, pp. 6759–6768.
- [77] A. H. Farzaneh and X. Qi, "Facial expression recognition in the wild via deep attentive center loss," in *Proceedings of the IEEE/CVF Winter Conference on Applications of Computer Vision*, 2021, pp. 2402–2411.
- [78] C. Shi, C. Tan, and L. Wang, "A facial expression recognition method based on a multibranch cross-connection convolutional neural network," *IEEE Access*, vol. 9, pp. 39 255–39 274, 2021.
- [79] A. P. Fard and M. H. Mahoor, "Ad-corre: Adaptive correlation-based loss for facial expression recognition in the wild," *IEEE Access*, vol. 10, pp. 26 756–26 768, 2022.
- [80] A. Graves, A.-r. Mohamed, and G. Hinton, "Speech recognition with deep recurrent neural networks," in *2013 IEEE international conference on acoustics, speech and signal processing*. Ieee, 2013, pp. 6645–6649.
- [81] J. Deng, W. Dong, R. Socher, L.-J. Li, K. Li, and L. Fei-Fei, "Imagenet: A large-scale hierarchical image database," in *2009 IEEE conference on computer vision and pattern recognition*. Ieee, 2009, pp. 248–255.
- [82] S. Rajan, P. Chenniappan, S. Devaraj, and N. Madian, "Novel deep learning model for facial expression recognition based on maximum boosted cnn and lstm," *IET Image Processing*, vol. 14, no. 7, pp. 1373–1381, 2020.
- [83] Z. Lian, Y. Li, J.-H. Tao, J. Huang, and M.-Y. Niu, "Expression analysis based on face regions in real-world conditions," *International Journal of Automation and Computing*, vol. 17, no. 1, pp. 96–107, 2020.
- [84] H. Li, N. Wang, X. Ding, X. Yang, and X. Gao, "Adaptively learning facial expression representation via cf labels and distillation," *IEEE Transactions on Image Processing*, vol. 30, pp. 2016–2028, 2021.
- [85] M. Galar, A. Fernández, E. Barrenechea, H. Bustince, and F. Herrera, "An overview of ensemble methods for binary classifiers in multi-class problems: Experimental study on one-vs-one and one-vs-all schemes," *Pattern Recognition*, vol. 44, no. 8, pp. 1761–1776, 2011.
- [86] Z. Wang, F. Zeng, S. Liu, and B. Zeng, "Oaenet: Oriented attention ensemble for accurate facial expression recognition," *Pattern Recognition*, vol. 112, p. 107694, 2021.
- [87] K. Wang, X. Peng, J. Yang, S. Lu, and Y. Qiao, "Suppressing uncertainties for large-scale facial expression recognition," in *Proceedings of the IEEE/CVF Conference on Computer Vision and Pattern Recognition*, 2020, pp. 6897–6906.
- [88] N. K. Benamara, M. Val-Calvo, J. R. Alvarez-Sanchez, A. Díaz-Morcillo, J. M. Ferrandez-Vicente, E. Fernández-Jover, and T. B. Stambouli, "Real-time facial expression recognition using smoothed deep neural network ensemble," *Integrated Computer-Aided Engineering*, no. Preprint, pp. 1–15, 2021.
- [89] X. Peng, Y. Gu, and P. Zhang, "Au-guided unsupervised domain-adaptive facial expression recognition," *Applied Sciences*, vol. 12, no. 9, p. 4366, 2022.
- [90] D. Ruan, Y. Yan, S. Chen, J.-H. Xue, and H. Wang, "Deep disturbance-disentangled learning for facial expression recognition," in *Proceedings of the 28th ACM International Conference on Multimedia*, 2020, pp. 2833–2841.
- [91] H. Yang, U. Ciftci, and L. Yin, "Facial expression recognition by de-expression residue learning," in *Proceedings of the IEEE conference on computer vision and pattern recognition*, 2018, pp. 2168–2177.
- [92] J. Zeng, S. Shan, and X. Chen, "Facial expression recognition with inconsistently annotated datasets," in *Proceedings of the European Conference on Computer Vision (ECCV)*, 2018, pp. 222–237.
- [93] X. Liu, B. Vijaya Kumar, J. You, and P. Jia, "Adaptive deep metric learning for identity-aware facial expression recognition," in *Proceedings of the IEEE conference on computer vision and pattern recognition workshops*, 2017, pp. 20–29.
- [94] V. Mavani, S. Raman, and K. P. Miyapuram, "Facial expression recognition using visual saliency and deep learning," in *Proceedings of the IEEE international conference on computer vision workshops*, 2017, pp. 2783–2788.
- [95] G. Bradski and A. Kaehler, "Opencv," *Dr. Dobb's journal of software tools*, vol. 3, 2000.
- [96] D. E. King, "Dlib-ml: A machine learning toolkit," *Journal of Machine Learning Research*, vol. 10, pp. 1755–1758, 2009.
- [97] C. Koch, "The role of the eyes and mouth in facial emotions," in *Abstracts of the Psychonomic Society*, vol. 10. Citeseer, 2005, p. 128.
- [98] C.-M. Kuo, S.-H. Lai, and M. Sarkis, "A compact deep learning model for robust facial expression recognition," in *Proceedings of the IEEE conference on computer vision and pattern recognition workshops*, 2018, pp. 2121–2129.